RESEARCH ARTICLE

Proteomic analysis reveals perturbed energy metabolism and elevated oxidative stress in hearts of rats with inborn low aerobic capacity

Jatin G. Burniston[1,2], Jenna Kenyani[3], Jonathan M. Wastling[3], Charles F. Burant[4], Nathan R. Qi[4], Lauren G. Koch[4,5] and Steven L. Britton[4,5]

[1] Research Institute for Sport and Exercise Sciences, Liverpool John Moores University, Liverpool, UK
[2] Institute for Health Research, Liverpool John Moores University, Liverpool, UK
[3] Institute of Infection and Global Health, University of Liverpool, Liverpool, UK
[4] Department of Internal Medicine, University of Michigan, Ann Arbor, MI, USA
[5] Department of Anesthesiology, University of Michigan, Ann Arbor, MI, USA

Received: September 17, 2010
Revised: May 5, 2011
Accepted: May 16, 2011

Selection on running capacity has created rat phenotypes of high-capacity runners (HCRs) that have enhanced cardiac function and low-capacity runners (LCRs) that exhibit risk factors of metabolic syndrome. We analysed hearts of HCRs and LCRs from generation 22 of selection using DIGE and identified proteins from MS database searches. The running capacity of HCRs was six-fold greater than LCRs. DIGE resolved 957 spots and proteins were unambiguously identified in 369 spots. Protein expression profiling detected 67 statistically significant ($p<0.05$; false discovery rate $<10\%$, calculated using q-values) differences between HCRs and LCRs. Hearts of HCR rats exhibited robust increases in the abundance of each enzyme of the β-oxidation pathway. In contrast, LCR hearts were characterised by the modulation of enzymes associated with ketone body or amino acid metabolism. LCRs also exhibited enhanced expression of antioxidant enzymes such as catalase and greater phosphorylation of α B-crystallin at serine 59, which is a common point of convergence in cardiac stress signalling. Thus, proteomic analysis revealed selection on low running capacity is associated with perturbations in cardiac energy metabolism and provided the first evidence that the LCR cardiac proteome is exposed to greater oxidative stress.

Keywords:
2-DE / Animal proteomics / Animal selection model / MS

1 Introduction

Divergent selection on running capacity has produced two populations of rats, high-capacity runners (HCRs) and low-capacity runners (LCRs), which have the potential to illuminate mechanisms underlying diseases associated with low cardiorespiratory fitness. Genetic heterogeneity of HCR-LCR lines is maintained by a rotational mating paradigm that minimises inbreeding [1], and concurrent breeding of LCRs and HCRs enables the lines to serve as reciprocal controls for unknown environmental changes. Compared with inbred strains, in which essentially all loci are fixed, these outbred selected lines maintain genetic complexity, allowing allelic variants to be enriched by selection pressure [2]. As a result, the HCR-LCR model is ideally suited to discovering the resultant effects of epistatic interactions, modifier genes or synergistic actions associated with different levels of aerobic capacity.

Sedentary HCRs and LCRs exhibit substantial differences in aerobic capacity, disease susceptibility and mortality rate. LCRs are relatively hypertensive, have poorer vascular function and higher fasting blood levels of glucose, insulin,

Correspondence: Dr. Jatin G. Burniston, Muscle Physiology and Proteomics Laboratory, Research Institute for Sport and Exercise Sciences, Tom Reilly Building, Liverpool John Moores University, Byrom Street, Liverpool L3 3AF, UK
E-mail: j.burniston@ljmu.ac.uk
Fax: +44-151-904-6284

Abbreviations: 4-HNE, 4-hydroxynonenal; **ACADL,** long-chain specific acyl-CoA dehydrogenase; **ACADS,** short-chain specific acyl-CoA dehydrogenase; **Acyl-CoA,** acyl-co-enzyme A; **ETD,** electron transfer dissociation; **FDR,** false discovery rate; **HCR,** high-capacity runner; **LCR,** low-capacity runner; **MAPK,** mitogen-activated protein kinase; **MTE-1,** mitochondrial thioesterase 1; **NADH,** nicotinamide adenine dinucleotide; **PPAR,** peroxisome proliferator activated receptor

triacylglycerides and free fatty acids [3]. LCRs are also more susceptible to environmental challenges such as ischaemia/reperfusion [4], high-fat diet [5] or hypoxia [6]. Exposure to hypoxia (7% oxygen) induces cardiac pump failure more rapidly in LCRs than HCRs [6]. That is, LCRs experience fatal irregular ventricular contractions within 8 min of hypoxia; in contrast, pump failure in HCRs occurs after 20 min of hypoxia and is characterised by a gradual diminution of cardiac systolic performance. At the cellular level, cardiomyocytes from LCRs are significantly shorter, contract less quickly and relax more slowly than those isolated from HCRs [6]. These differences are accompanied by greater expression of β-myosin heavy chain and differences in Ca^{++} transients, but the expression of proteins associated with Ca^{++} handling; sarco-endoplasmic reticulum ATPase, phospholamban, Na^{+}–Ca^{++} exchanger or calsequestrin is similar in LCR and HCR hearts [6]. Therefore, the mechanisms responsible for contractile dysfunction associated with selection on low running capacity are not yet fully understood.

Molecular differences that regress with low running capacity may provide further mechanistic insight to the elevated disease risk and cardiac dysfunction observed in LCR rats and individuals with low aerobic capacity. Microarray analysis [7] of HCR-LCR hearts detected 1540 differences in gene expression and highlighted enrichment of genes involved in lipid metabolism in HCRs, whereas glucose metabolism and microtubule-based processes were enriched in LCRs. However, alterations in gene expression do not necessarily result in concomitant changes in protein abundance and post-translational processes can give rise to protein species that are undetectable in microarray analyses. The protein complement of a cell (i.e. its proteome) defines that cell and dictates its functional characteristics. Therefore, it is of mechanistic value to verify if the differences in gene expression are also evident at the protein level, and determine protein modifications that regress with differences in running capacity.

2 Materials and methods

2.1 Animal model

The inception of HCR-LCR strains from a founder population of genetically heterogeneous N:NIH rats has been described in detail [1]. In the current work, hearts from adult male HCR and LCR rats ($n = 6$ in each group) from generation 22 were used. Animals were housed (two per cage) in accordance with the University of Michigan Committee guidelines on the use and care of animals. Environmental conditions were $20 \pm 2^{\circ}C$, 40–50% relative humidity with a 12 h light (0600–1800) and dark cycle. Food and water were available ad libitum. Home cage activity was measured gravimetrically during a 72 h period, as described previously [8]. Non-fasting blood samples were collected prior to the animals being killed. Serum glucose levels were measured using an Accu-Chek glucose meter (Roche Diagnostics, Basel, Switzerland), serum insulin concentrations were determined by ELISA using a commercially available rodent assay (Linco Research, St. Charles, MO, USA).

2.2 Muscle processing

Animals were killed by cervical dislocation and their hearts isolated and washed with saline before being blotted dry and weighed. Cardiac septa were pulverised in liquid nitrogen then homogenised on ice in lysis buffer: 7 M urea, 2 M thiourea, 4% w/v CHAPS, 30 mM Tris, pH 8.5, at 4°C, containing Complete™ protease inhibitor (Roche Diagnostics). After centrifugation at $12\,000 \times g$, 4°C for 45 min supernatants were decanted, precipitated in acetone and resuspended in DIGE lysis buffer. Insoluble proteins were incubated in 1% v/v SDS and at 90°C for 30 min then washed twice in 0.1% w/v Rapigest SF (Waters; Milford, MA, USA) in 50 mM ammonium bicarbonate using 5 kDa M_r cut-off spin columns. Protein suspensions were concentrated to ~50 μL, then incubated at 80°C for 15 min. DTT was added (final concentration 1 mM) and incubated at 60°C for 15 min followed by incubation in the presence of 5 mM iodoacetamide at 4°C, protected from light. Sequencing grade trypsin (Promega; Madison, WI, USA) was added at a protein ratio of ~1:50 and digestion allowed to proceed at 37°C overnight. Digestion was terminated by the addition of 2 μL concentrated HCl and peptide solutions centrifuged at $13\,000 \times g$ for 5 min to clear supernatants in preparation for iTRAQ labelling and LC-MALDI-MS.

The protein/peptide concentrations were measured using the Bradford assay (Sigma, Poole, Dorset, UK). Samples prepared for DIGE were adjusted to 5 μg/μL in lysis buffer.

2.3 DIGE of soluble cardiac proteins

Fifty microgram aliquots of each sample and the pooled internal standard were labelled with 400 pmol CyDye DIGE Fluor minimal dyes (GE Healthcare, Chalfont St. Giles, UK), consistent with previous work [9]. Cy3 and Cy5 labelling was alternated between LCR and HCR samples in a 'balanced' design. Labelled LCR and HCR aliquots and pooled Cy2-labelled standard were combined with rehydration buffer: 7 M urea, 2 M thiourea, 2% w/v CHAPS, 20 mM DTT and 0.5% v/v ampholytes. IPG strips (24 cm, pH 3–11, non-linear; Immoboline Drystrip, GE Healthcare) were rehydrated overnight in 450 μL rehydration buffer that contained the combined Cyanine-labelled samples. Isoelectric focusing (maximum 50 μA per strip) was performed on an IPGPhor II (GE Healthcare) at 20°C using the protocol (total 44 000 Vh): 3 h at 300 V, 3 h at 600 V, 3 h at 1000 V, gradient to 8000 V in 3 h then 4 h at 8000 V. IPG strips were equilibrated in 50 mM Tris-HCl, pH 8.8, containing 6 M urea, 30% v/v glycerol, 2% w/v SDS and bromophenol blue.

DTT (10 mg/mL) was present in the first equilibration and iodoacetamide (25 mg/mL) in the second. Proteins were electrophoresed (Ettan Dalt six; GE healthcare) through denaturing 12.5% polyacrylamide gels at 20°C; at 5 W per gel for 30 min, then 17 W per gel until the tracking dye reached the bottom edge.

2.4 SameSpots protein expression profiling

Gels were digitised (16-bit greyscale, 100 μm pixel size) immediately after electrophoresis using a fluorescence scanner (Typhoon 9400, GE Healthcare) at wavelengths appropriate for Cy2, Cy3 and Cy5 dyes. Gel images (Cy2, Cy3 and Cy5, total = 18) were aligned using SameSpots (Nonlinear Dynamics, Newcastle, UK). Prominent spots (mean ± SD per gel image: 548 ± 36) were used as vectors to warp each image to a common reference gel. A mask was used to remove gel artefacts (109 spots deleted) and features with an average normalised volume <10 000 (147 spots) or spot area <150 (33 spots) were disregarded. In total, 957 spots were included in the subsequent statistical analysis. As a measure of technical variation, when ranked by coefficient of variation, 70% of spots in Cy2 images (pooled standard) had a coefficient of variation <14%.

Log-transformed spot volumes, expressed relative to the pooled standard, were used to investigate differences in expression between LCR and HCR groups by one-way analysis of variance. To control false discovery rate (FDR), the *p*-value distribution was used to calculate *q*-values and a criterion FDR of 10% was set. This statistical approach, which considers the biological variation across each spot, is more sophisticated than arbitrary implementation of a threshold based on fold-change. Associations between serum insulin levels and differentially expressed spots (i.e. $p<0.05$, FDR <10%) were investigated by Pearson correlation of HCR and LCR data using Prism 4.0 (GraphPad Software, La Jolla, CA, USA).

2.5 Identification of gel spots using MALDI-MS/MS and ESI-MS/MS

Spots were robotically excised from colloidal Coomassie-stained (Bio-Safe; Bio-Rad, Hercules, CA, USA) preparative gels loaded with 1.5 mg protein (pooled standard) and proteins identified by MALDI-MS/MS analysis of in-gel tryptic digests, as described previously [10]. Peak lists were searched against the Swiss-Prot database (57.1) restricted to 'Rattus' (7347 sequences) using a locally implemented MASCOT (www.matrixscience.com) server (version 2.2.03). The enzyme specificity was trypsin allowing one missed cleavage, carbamidomethyl modification of cysteine (fixed), oxidation of methionine (variable) and an *m/z* error of ±0.5 Da. Identification was accepted based on a significant MOWSE score; the threshold ($p<0.05$) was 51 using the described database constraints. Up to three confirmatory MS/MS spectra were automatically acquired from digests with MOWSE scores <120. Selection of MS/MS fragment ion spectra (average *m/z*) was restricted to 42 ions over six segments encompassing 5–95% of the precursor ion *m/z*. MS/MS ion lists were searched against the Swiss-Prot database (tolerance ±0.5 Da parent, ±0.8 Da fragments) using the constraints described for peptide mass fingerprinting.

Selected spots were analysed using nano LC-ESI-MS/MS. Tandem electrospray mass spectra were recorded using a quadrupole-high capacity ion-trap (HCT Ultra ETD II; Bruker Daltonics, Bremen, Germany) coupled to a nano-flow HPLC system (Ultimate 3000; Dionex, Sunnyvale, CA, USA). Five microlitres of sample (in-gel digest) was injected and peptides eluted using an ACN/0.1% formic acid gradient of 2–40% B in 30 min at a flow rate of 300 nL/min (column Acclaim PepMap 100, C18, 3 μm, 100 Å, 75 μm × 15 cm, Dionex). An online nanospray source (Bruker Daltonics) was used equipped with a fused silica emitter (PicoTip FS360-20-10-D, New Objective). The capillary voltage was–1300 V and a survey scan from *m/z* 300 to 1500 was used to select peptides with charge states of +2 or +3 using Enhanced Scan mode (8100 (*m/z*)/s). Data-dependent MS/MS analysis in alternating CID/electron transfer dissociation (ETD) mode was performed selecting the two most abundant precursor ions with active exclusion enabled. Data were searched against the Swiss-Prot database (tolerance ±1.3 Da parent, ±0.5 Da fragments) using the constraints described for peptide mass fingerprinting with phosphorylation of serine, threonine or tyrosine residues as possible modifications.

2.6 Analysis of insoluble cardiac proteins using iTRAQ and LC-MALDI-MS/MS

Ten microgram aliquots of LCR and HCR samples and pooled internal standard were labelled with iTRAQ reagents according to the manufacturer's instructions (Applied Biosystems; Foster City, CA, USA). HCR and LCR samples were labelled with iTRAQ 114, 115 or 116 in a 'balanced' design and combined with the pooled standard labelled with iTRAQ 117 to produce 4-plex experiments. Samples, labelled with iTRAQ reagents, were analysed in triplicate, as described previously [11]. LC-MALDI automation software selected 500 precursors in order of descending intensity from chromatographic peaks of at least 20 s width. MS/MS spectra were analysed for protein identification and parsed with spectra of iTRAQ reporter ions (*m/z* 114, 115, 116 and 117) collected using the instrument's low-mass zoom feature. Data were searched against the Swiss-Prot database using the constraints described for peptide mass fingerprinting with the addition of quantitation (iTRAQ 4-plex) as a possible modification. Proteins with two or more iTRAQ peptides with ions scores greater than the identity threshold were selected for quantitation. Data expressed relative to the

pooled internal standard were averaged from triplicate analyses to create protein lists for each animal. Statistically significant differences were determined using log-transformed expression data.

2.7 Muscle enzyme activity

β-(3)-Hydroxyacyl-CoA dehydrogenase activity was measured in muscle homogenates prepared in 100 mM K_2HPO_4 and 2 mM EDTA, pH 7.3 [12]. Homogenates were diluted in 100 mM K_2HPO_4, pH 7.3 containing 6.4 mM β-nicotinamide adenine dinucleotide (NADH) and mixed with 5.4 mM *S*-acetoacetyl-CoA to a final concentration of 97 mM K_2HPO_4, 0.1 mM β-NADH, 0.09 mM *S*-acetoacetyl-CoA. The rate of disappearance of NADH was determined by measuring the change in absorbance at 340 nm for 5 min at 37°C.

2.8 Western blot analysis

Muscle powders were homogenised on ice in 1% w/v SDS containing Complete™ protease inhibitor (Roche Diagnostics) and centrifuged at 12 000 × *g*, 4°C for 20 min. Supernatants were adjusted to 5 μg/μL protein in 2 × Laemmli buffer and incubated at 90°C for 5 min. Seventy-five microgram aliquots of HCR and LCR proteins were separated by SDS-PAGE and electro-transferred to PVDF membranes. For immunoblotting of 2-DE gels, 500 μg protein prepared for preparative gels was loaded on 13 cm, pH 3–10, IPG strips (GE Healthcare) and transferred to PVDF membranes as described previously [13]. Membranes were blocked with 5% non-fat dried milk in 0.05% v/v Tween-20 in PBS then incubated overnight at 4°C with primary antibodies specific for either 4-hydroxynonenal (4-HNE; 1:1000 ab46544; Abcam, UK), α B-crystallin (1:10000 ab13497; ABcam) or α B-crystallin phosphorylated at serine 59 (1:2000 ab5577; Abcam) in 1% non-fat dried milk Tween-20 in PBS. Secondary antibodies were from Abcam (ab6741 (1:5000) and ab6721 (1:3000)) and immunoreactive proteins were detected by ECL (ECL Prime, GE Healthcare) and quantified by densitometry. Equivalent transfer of proteins was assessed by post-staining PVDF membranes with Ponceau S or Direct Blue 71.

2.9 On-membrane MALDI-MS/MS

Protein spots visualised by anti-4-HNE immunoblotting after 2-DE were identified by on-membrane MALDI-MS/MS. Membranes were striped by incubation (45 min at 50°C) in 100 mM DTT, 2% w/v SDS 52.5 mM Tris, pH 6.7, and affixed to MALDI target plates using conductive tape. Sequencing grade modified trypsin (0.2 μg/μL in 25 mM Ammonium bicarbonate; Promega) was dispensed at the positions (*x*, *y* coordinates) of immunoreactive proteins and prominent 'landmark' spots using a piezoelectric printing device (ChIP, Chemical Inkjet printer, Shimadzu Biotech). One nano-litre spots were printed (ten intervals of 100 pL) at a spacing of 500 μm within the border of each protein position and on-membrane digestion was allowed to proceed overnight at 37°C in a humidified chamber. Spot positions were over-printed (2 nL spots dispensed in intervals of 100 pL) with matrix solution (5 μg/μL CHCA in 50:50 ACN and 0.1% TFA) and a calibration mix (Proteomass; Sigma) consisting of bradykinin (*m/z* 756.39), angiotensin II (*m/z* 1046.54), P14R (*m/z* 1533.85) and adrenocorticotropic hormone (ACTH) fragment (*m/z* 2465.19) was pipetted (0.5 μL) in the target-plate calibration wells and overlaid with 0.5 μL matrix solution. Membranes were dried at 37°C for 1 h prior to MALDI-MS/MS analysis directed at each protein coordinate. Data were searched against the Swiss-Prot database using the constraints described for peptide mass fingerprinting.

3 Results

3.1 Exercise capacity of HCRs and LCRs

Rats in the founder population ran 355 ± 11 m during a standardised run to exhaustion on a motorised treadmill [1]. Using an identical procedure, HCR rats from generation 22 ran 6.2-fold further than LCRs when they were 3 months old (1864 ± 40 versus 299 ± 6 m) and four-fold further (754 ± 24 versus 185 ± 10 m) prior to isolation of the hearts at 12 months of age. At each assessment HCRs performed significantly more running work compared with LCRs. Habitual cage activity during either light or dark periods was not significantly different in HCRs and LCRs (Supporting Information Table 1). Serum glucose (mg/dL) was not different (196.3 ± 23 in HCRs versus 195.3 ± 22 in LCRs) whereas serum insulin (ng/mL) was significantly ($p < 0.0001$) greater in LCRs (4.84 ± 0.5) compared with HCRs (1.32 ± 0.2). Gross and lean body weights of HCRs were less than LCRs and the absolute wet weight of the hearts was significantly greater in HCRs, equating to a 1.5-fold greater heart: lean body mass ratio (Supporting Information Table 1).

3.2 DIGE analysis of soluble cardiac proteins

Differential analysis was performed on 957 spots and the expression of 67 gel spots was significantly (FDR < 10%) different between HCRs and LCRs. MS unambiguously identified proteins in 369 gel spots (Supporting Information Table 2), including 56 of the differentially expressed spots. A 2-D gel map of the proteins identified by MS is available in the World 2D-PAGE repository (http://world-2dpage.expasy.org/repository/), accession number 0022 and a representative pseudo-colour image of the DIGE separation is

available online (Supporting Information Fig. 1). This proteome mining work revealed majority of proteins were resolved as multi-spot series. Thus, the 369 identified gel-spots comprise 170 gene products and, in total, DIGE and MS analysis identified 39 gene products that were differentially expressed between HCRs and LCRs (Table 1). Further to differences between HCR and LCR group means, significant correlation was found between individual serum insulin concentrations in LCRs and the abundance of coronin-6 (spot 1; $R^2 = 0.7410$, $p = 0.0277$) and propionyl-CoA carboxylase α-chain (spot 23; R^2 0.662, $p = 0.0489$) whereas low serum insulin levels in HCRs correlated with the abundance of hydroxyacyl-CoA dehydrogenase (spot 80; $R^2 = 0.907$, $p = 0.0034$), succinyl-CoA: 3-ketoacid coenzyme A ($R^2 = 0.8587$, $p = 0.0079$), ventricular myosin regulatory light chain (spot 83; $R^2 = 0.8295$, $p = 0.0116$) and protein disulfide-isomerase A3 (Spot 45; $R^2 = 0.6869$, $p = 0.0415$).

3.3 iTRAQ analysis of insoluble cardiac proteins

Twenty-eight proteins met the inclusion criteria for iTRAQ analysis (Supporting Information Table 3) and the expression of six proteins differed significantly ($p < 0.05$) between HCRs and LCRs (Table 2). iTRAQ detected 11 gene products (3-keto acyl-co-enzyme A (acyl-CoA) thiolase, ADP/ATP translocase 1, citrate synthase, cytochrome *c* oxidase subunit 4 isoform 1, cytochrome *c* oxidase subunit 5A, cytoplasmic dynein, fatty acid-binding protein, haemoglobin subunit α-1/2, haemoglobin subunit β-1, myosin-6 and myosin-7) not observed using DIGE. Four of these proteins (3-keto acyl-CoA thiolase, ADP/ATP translocase 1, cytochrome *c* oxidase subunit 4 isoform 1 and cytochrome *c* oxidase subunit 5A) were differentially expressed between HCRs and LCRs. Three proteins (ATP synthase subunit α, isocitrate dehydrogenase and myosin regulatory light chain 2) identified as differentially expressed using DIGE were also detected in the iTRAQ analysis. In each case no significant difference was detected using iTRAQ, which is consistent with our previous experience [11].

3.4 Biochemical and immunoblot analyses

The proteomic analyses point to differences in β-oxidation of fatty acids and exposure to oxidative stress. β-(3)-Hydroxyacyl-CoA dehydrogenase activity is commonly used as a measure of β-oxidation capacity and was 1.3-fold greater in HCR (75.4 ± 3.3 versus 56.7 ± 3.3 μmol/g/min, $p = 0.002$), whereas proteins associated with exposure to H_2O_2 and lipid peroxidation, such as 4-HNE, were detected in LCR hearts. Western blotting detected a prominent 4-HNE-reactive band at ~45 kDa that was significantly ($p = 0.015$) more abundant in LCRs (Fig. 1). Immunoblot analysis of 2-DE separated proteins revealed two 4-HNE immunoreactive spots in LCR hearts (Fig. 1D), which were each identified as long-chain specific acyl-CoA dehydrogenase (ACADL) and correspond to spots 651 and 627 of the DIGE map. α B-crystallin is an abundant small heat shock protein in cardiac muscle and was resolved as three discrete isoelectric species (spots 20, 640 and 717) using DIGE. Spot 20 was 1.67-fold greater in LCRs and nano flow liquid chromatography (nLC)-ESI-MS/MS revealed this spot contained peptides phosphorylated at S^{59} that were not present in spot 640 or 717 (Fig. 2). Western blotting further confirmed the ratio of phosphorylated (S^{59}) to total α B-crystallin was significantly greater in LCRs (Fig. 2F).

4 Discussion

Proteomic analysis revealed selection on running capacity is associated with changes in cardiac energy metabolism and discovered the first evidence that the cardiac proteome of LCRs is exposed to greater oxidative stress. These findings closely support the conclusions of our [7] microarray investigation but, in the majority, proteomic analysis discovered new information rather than simply providing protein-level confirmation of earlier reported [7] differences in gene expression. The limited direct correspondence between proteome and transcriptome data is, in part, due to the larger number of genes assayed by microarray compared to DIGE. In addition, it is important to recognise the majority of proteins were resolved as multiple spots using 2-DE; therefore, differences in spot expression may indicate differences in post-translational modification and provide information not evident at the transcriptome level.

The current work revealed conspicuous differences in β-oxidation enzymes suggesting an enhanced capacity for fatty acid oxidation in HCRs. Specifically, DIGE detected pronounced modulation of each enzyme of the matrix component of the β-oxidation pathway (Table 1) responsible for oxidation of short-chain fatty acyl-CoA [14]. Accordingly, β-hydroxyacyl-CoA dehydrogenase activity was significantly greater in HCRs and the abundance of this key enzyme closely correlated with low serum insulin concentrations in these animals. Modulation of short-chain specific acyl-CoA dehydrogenase (ACADS) was a prominent feature in the current analysis. ACADS was observed as multiple spots (4, 10, 11 and 14) and the abundance of the most basic species (spot 11) was two-fold greater in LCRs, whereas, spots 4, 10 and 14 were two-fold greater in HCRs. These isoelectric species may represent different post-translational states, for example phosphorylated species of ACADS have been reported [15]. In the current work nLC-ESI-MS/MS analysis identified 84% of the ACADS sequence (57 unique peptides, MOWSE score = 2806), but did not include phosphorylated residues. Nonetheless, the ACADS spot pattern in HCRs closely resembles that of endurance-trained rats [10], and putative post-translational modulation of ACADS is a consistent feature associated with changes in cardiac performance. For example, genetic deletion of phospholamban, which produces a hyper-dynamic cardiac

Table 1. DIGE expression data

Description	Protein ID	Ref#	HCR norm. vol.	LCR norm. vol.	Fold diff.
Energy metabolism					
Fatty acid metabolism					
Short-chain specific acyl-CoA dehydrogenase	P15651	11	0.741±0.018	1.517±0.167	+2.05
Short-chain specific acyl-CoA dehydrogenase	P15651	4	1.432±0.038	0.594±0.232	−2.41
Short-chain specific acyl-CoA dehydrogenase	P15651	10	1.409±0.055	0.665±0.196	−2.12
Short-chain specific acyl-CoA dehydrogenase	P15651	14	1.198±0.056	0.668±0.118	−1.79
Enoyl-CoA hydratase, mitochondrial	P14604	105	1.138±0.016	0.971±0.01	−1.17
Enoyl-CoA hydratase, mitochondrial	P14604	127	1.021±0.019	0.89±0.021	−1.15
Enoyl-CoA hydratase, mitochondrial	P14604	174	0.963±0.017	0.88±0.013	−1.09
Hydroxyacyl-CoA dehydrogenase	Q9WVK7	80	1.378±0.052	1.130±0.048	−1.22
Hydroxyacyl-CoA dehydrogenase	Q9WVK7	143	1.175±0.011	1.039±0.036	−1.13
Acyl-coenzyme A thioesterase 2	O55171	30	1.104±0.056	0.7±0.077	−1.58
Acyl-coenzyme A thioesterase 2	O55171	61	1.113±0.033	0.878±0.023	−1.27
Amino acid degradation					
Propionyl-CoA carboxylase α chain	P14882	22	1.422±0.052	0.861±0.083	−1.65
Propionyl-CoA carboxylase α chain	P14882	23	0.873±0.115	1.421±0.043	+1.63
δ-1-Pyrroline-5-carboxylate dehydrogenase	P0C2X9	29	0.815±0.049	1.293±0.051	+1.59
Methylcrotonoyl-CoA carboxylase subunit α	Q5I0C3	53	0.841±0.029	1.098±0.067	+1.31
Ketone body metabolism					
Succinyl-CoA:3-ketoacid-coenzyme A transferase 1	B2GV06	17	0.941±0.088	1.628±0.215	+1.73
Acetyl-CoA acetyltransferase	P17764	41	1.33±0.065	0.92±0.066	−1.45
Acetyl-CoA acetyltransferase	P17764	152	0.965±0.015	1.082±0.024	+1.21
Glycolytic metabolism					
Dihydrolipoyllysine-residue acetyltransferase component of pyruvate dehydrogenase complex	P08461	147	1.053±0.018	0.935±0.028	−1.13
Glycogen phosphorylase, muscle form	P09812	47	1.117±0.085	0.805±0.051	−1.39
Tricarboxylic acid cycle					
Fumarate hydratase, mitochondrial	P14408	5	1.478±0.067	0.620±0.147	−2.38
Fumarate hydratase, mitochondrial	P14408	6	1.516±0.062	0.649±0.146	−2.33
Isocitrate dehydrogenase (NADP)	P56574	129	0.987±0.033	1.131±0.018	+1.15
2-Oxoglutarate dehydrogenase E1 component	Q5XI78	70	0.977±0.043	1.218±0.041	+1.25
Electron transport chain					
Succinate dehydrogenase [ubiquinone] iron-sulfur subunit	P21913	182	1.097±0.005	1.073±0.006	−1.02
Electron transfer flavoprotein subunit α	P13803	121	0.975±0.021	0.843±0.032	−1.16
Electron transfer flavoprotein-ubiquinone oxidoreductase	Q6UPE1	91	0.994±0.041	0.835±0.028	−1.19
Cytochrome b-c1 complex subunit 2	P32551	77	1.197±0.039	0.979±0.041	−1.22
ATP synthase subunit α	P15999	164	0.994±0.009	1.099±0.027	+1.11
Voltage-dependent anion-selective channel protein 1	Q9Z2L0	137	0.996±0.026	0.876±0.023	−1.14
Antioxidant/stress response					
Catalase	P04762	19	0.713±0.049	1.212±0.053	+1.70
Catalase	P04762	42	0.932±0.072	1.329±0.073	+1.43
Aldehyde dehydrogenase 2	P11884	124	0.92±0.028	1.058±0.033	+1.15
Glutathione *S*-transferase Mu 2	P08010	2	1.618±0.189	0.542±0.167	−2.99
Protein disulfide-isomerase A3	P11598	13	1.472±0.062	0.799±0.15	−1.84
Protein disulfide-isomerase A3	P11598	37	1.222±0.054	0.809±0.096	−1.51
Protein disulfide-isomerase A3	P11598	45	1.262±0.069	0.909±0.055	−1.39
Heat shock protein β-7 (Fragment)	Q9QUK5	7	1.419±0.259	0.61±0.057	−2.33
α-Crystallin B chain	P23928	20	0.768±0.094	1.282±0.133	+1.67
Myofibrillar and cytoskeletal					
Myosin regulatory light chain 2, ventricular/cardiac muscle	P08733	66	0.988±0.031	1.245±0.038	+1.26
Myosin regulatory light chain 2, ventricular/cardiac muscle	P08733	83	0.950±0.041	1.15±0.043	+1.21
Desmin	P48675	60	0.88±0.03	1.118±0.049	+1.27
Desmin	P48675	169	1.022±0.02	1.125±0.023	+1.10
Vimentin	P31000	15	1.373±0.222	0.771±0.044	−1.78
EH domain-containing protein 1	Q641Z6	25	0.755±0.044	1.213±0.029	+1.61
EH domain-containing protein 1	Q641Z6	50	0.861±0.036	1.147±0.025	+1.33

Table 1. Continued

Description	Protein ID	Ref#	HCR norm. vol.	LCR norm. vol.	Fold diff.
Coronin-6	Q920J3	1	0.446±0.046	1.972±0.485	+4.42
Rab GDP dissociation inhibitor α	P50398	56	1.149±0.054	0.898±0.047	−1.28
PDZ and LIM domain protein 1	P52944	64	1.054±0.036	0.835±0.049	−1.26
Miscellaneous					
Annexin A3	P14669	150	1.053±0.029	0.937±0.022	−1.12
Apolipoprotein E	P02650	89	0.903±0.041	1.076±0.019	+1.19
Prostaglandin reductase 2	Q5BK81	9	1.673±0.221	0.733±0.188	−2.28
Proteasome activator complex subunit 1	Q63797	133	0.859±0.01	0.98±0.033	+1.14
Pyridoxine-5′-phosphate oxidase	O88794	39	1.443±0.043	0.99±0.14	−1.46

Protein description and Protein ID relate to the Swiss-Prot database (57.1) entry identified from MASCOT searches of MS and MS/MS spectra. HCR and LCR expression ratios are average±SD relative to the pooled internal standard. Fold difference relative to HCR values are reported for spots exhibiting significant ($p<0.05$) differences in expression at an FDR of <10%.

Table 2. iTRAQ analysis of insoluble protein fraction

Description	Swiss-Prot ID	MOWSE	HCR	LCR	Difference (*p*-value)
3-Ketoacyl-CoA thiolase, mitochondrial	P13437	70±4	1.690±0.665	0.903±0.165	−1.872 (0.01)
ADP/ATP translocase 1	Q05962	119±12	1.802±0.856	0.72±0.253	−2.503 (0.025)
Cytochrome b-c1 complex subunit 1, mitochondrial	Q68FY0	79±24	1.053±0.088	0.553±0.229	−1.904 (0.003)
Cytochrome *c* oxidase subunit 4 isoform 1, mitochondrial	P10888	70±4	1.258±0.164	0.748±0.374	−1.682 (0.024)
Cytochrome *c* oxidase subunit 5A, mitochondrial	P11240	69±5	1.170±0.198	0.702±0.313	−1.667 (0.023)
Tropomyosin α-1 chain	P04692	159±49	0.540±0.277	1.060±0.153	+1.963 (0.01)

Protein description, database name and ID relate to the Swiss-Prot database (57.1) entry returned using the MASCOT search engine. A MOWSE score greater than 51 denotes a confident ($p<0.05$) protein identification. HCR and LCR expression ratios are the average±SD of peptides quantified in each sample expressed relative to the pooled internal standard. Fold difference relative to HCR values is reported and *p*-values were determined from log-transformed data using Student's independent *t*-tests. The complete list of proteins identified by iTRAQ and the average±SD number of MS/MS ions analysed and the average±SD peptides that met the inclusion criteria for iTRAQ analysis (including amino acid sequences identified) are reported in Supporting Information Table 3.

phenotype, is associated with a similar shift in ACADS spot pattern [16], and elevated expression of low-p*I* ACADS spots in hearts of swim-trained rats correlates with enhanced ACADS activity [17].

Differential expression of β-oxidation enzymes coincided with differences in electron transfer proteins and components of the respiratory chain. This may indicate tighter coupling specifically between β-oxidation of short-chain fatty acyl-CoA and oxidative phosphorylation that is important for enhanced aerobic capacity. Acyl-CoA dehydrogenases reduce flavin adenine dinucleotide (FADH2) and transfer electrons to electron transfer flavoprotein-ubiquinone oxidoreductase via electron transfer flavoprotein-α, driving the reduction of ubiquinone. Both electron transfer flavoprotein-α and electron transfer flavoprotein-ubiquinone oxidoreductase were identified as multi-spot series and the expression of individual spots within these series was significantly different in HCR and LCR hearts. In addition, subunit 2 of cytochrome b-c1, was 1.22-fold less in LCRs and iTRAQ detected 1.9-fold lower abundance of subunit 1 of cytochrome b-c1 and ~1.67-fold lesser abundance of cytochrome *c* oxidase subunits 4 and 5A in LCRs. These findings are consistent with enrichment of fatty acid oxidation genes reported in the HCR transcriptome. Furthermore, DIGE provided protein-level confirmation of the elevated mRNA expression of acyl-CoA thioesterase 2 (mitochondrial thioesterase 1: MTE-1) in HCRs [7]. MTE-1 hydrolyses fatty acyl-CoA to its free fatty acid anion, which may be exported from the mitochondrion [18]. MTE-1 is also modulated in endurance-trained hearts [10] and this adaptation may serve to protect the inner mitochondrial membrane by preventing accumulation of acyl-carnitine, which is a strong surfactant and can damage lipid membranes [19].

The observed differences in metabolic enzymes may be related to impaired peroxisome proliferator activated receptor (PPAR)-α signalling in LCRs. The PPAR gene ontology pathway was overrepresented in microarray analysis [7] of HCR-LCR hearts, and some genes of the modulated proteins involved in β-oxidation (Table 1) have PPAR-responsive elements [20]. Interestingly, metabolomic profiling of PPARα$^{-/-}$ mice [21] reveals a compensatory increase in leucine metabolism. Degradation of branched-

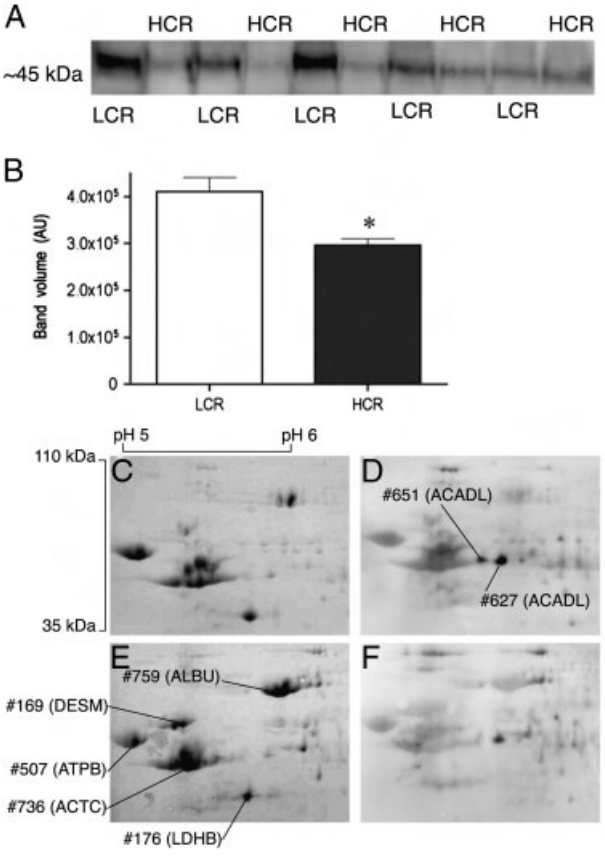

Figure 1. 4-HNE modification of ACADL. Western blot analysis (A) of 4-HNE-modified proteins detected a prominent band at 45–50 kDa that was more abundant in LCR hearts (B). Homogenates of LCR (C and D) and HCR (E and F) hearts were separated by 2-DE and transferred to PVDF membranes. Proteins were visualised by Ponceau S staining (C and E) or immunoblot analysis of 4-HNE-modified residues (D and F). 4-HNE immunoreactive spots and prominent spots stained by Direct Blue 71 were identified by MS analysis of on-membrane tryptic digests. Two 4-HNE immunoreactive spots, corresponding to #651 and #627 of the DIGE map, were more intensely labelled in LCR hearts (D) and were identified as ACADL.

chain amino acids, in particular leucine, is ketogenic and DIGE detected modulation of methylcortonyl-CoA carboxylase subunit-α and propionyl-CoA carboxylase α-chain, which contribute to branched-chain amino acid degradation or β-oxidation of odd chain-length and methyl-branched fatty acyl-CoA. Moreover, succinyl-CoA: 3-ketoacid-coenzyme A transferase 1 (spot 17), which catalyses the rate-limiting step in ketolysis, was more abundant in LCR hearts and low serum insulin concentrations in HCRs correlated with low abundance of this enzyme. The second reaction in ketolysis is catalysed by acetyl-CoA acetyltransferase and this protein was detected in two spots, the abundance of spot 41 was 1.5-fold less, whereas, spot 152 was 1.2-fold greater in LCRs suggesting a shift in post-translational state of this enzyme. As yet, it is not possible to determine whether these findings depict altered amino acid degradation only, or concurrent differences in ketone body and amino acid degradation in LCRs.

The lesser abundance of β-oxidation and electron transport chain enzymes in LCRs indicates diminished mitochondrial capacity, which may be associated with greater oxidative stress and H_2O_2 production that can cause irreversible damage to macromolecules. Indeed, catalase, which scavenges H_2O_2, was significantly more abundant in LCRs and two proteins, aldehyde dehydrogenase-2 and glutathione *S*-transferase, that defend against lipid peroxidation products such as 4-HNE were also differentially expressed. Phosphorylation of aldehyde dehydrogenase-2 protects against ischaemic damage to the heart [22] and this protein was modulated in a manner suggesting post-translational modification in LCRs, whereas, glutathione *S*-transferase was less abundant in LCRs, which is consistent with findings in hearts of spontaneously hypertensive rats [23]. Thyfault et al. [24] report elevated catalase activity and higher levels of 4-HNE-modified proteins associated with hepatic steatosis in LCRs. Using a similar approach, we detected a greater abundance of 4-HNE-modified ACADL in LCR heart (Fig. 1), which may be linked to the observed modulation of enzymes specifically responsible for β-oxidation of short-chain fatty acids. Recently, Tweedie et al. [25] reported greater activity of catalase and superoxide dismutase in skeletal muscle of HCR, which is in contrast to the findings in heart and liver. In the current work, superoxide dismutase and other key enzymes of the antioxidant defense system, including glutathione peroxidase, were detected by DIGE but were not different between HCRs and LCRs.

Selection on running capacity resulted in differential expression of chaperone proteins, including protein disulfide isomerase A3, heat shock protein β-7 (cardiovascular heat shock protein) and α B-crystallin. The expression of cardiovascular heat shock protein was 2.33-fold less in LCRs and protein disulfide isomerase A3, which was resolved as three spots, was on average 1.6-fold less in LCRs. αB-crystallin was also resolved as three spots (20, 640 and 717) and the abundance of phosphorylated (S^{59}) α B-crystallin (spot 20) was 1.67-fold greater in LCRs (Fig. 2). Phosphorylation of α B-crystallin at S^{59} is associated with protection against a variety of different environmental stresses. For example, exposure of cardiomyoblasts to H_2O_2 activates the p38 mitogen-activated protein kinase (MAPK)/mitogen and stress-activated protein kinase 1 pathway resulting in phosphorylation of α B-crystallin S^{59} [26]; similarly ischaemia/reperfusion injury activates p38 MAPK and is associated with S^{59} phosphorylation [27]. Therefore, the greater phosphorylation of α B-crystallin S^{59} observed here (Fig. 2) is consistent with enrichment of the stress-activated p38 MAPK signalling in the LCR cardiac transcriptome [7].

Phosphorylated α B-crystallin is also associated with cytoskeletal stress whereupon this chaperone translocates and interacts with desmin [28]. Elevated expression of desmin is a feature of human cardiomyopathy [29] and was also observed in LCR hearts (Table 1). Moreover, cytoskeletal

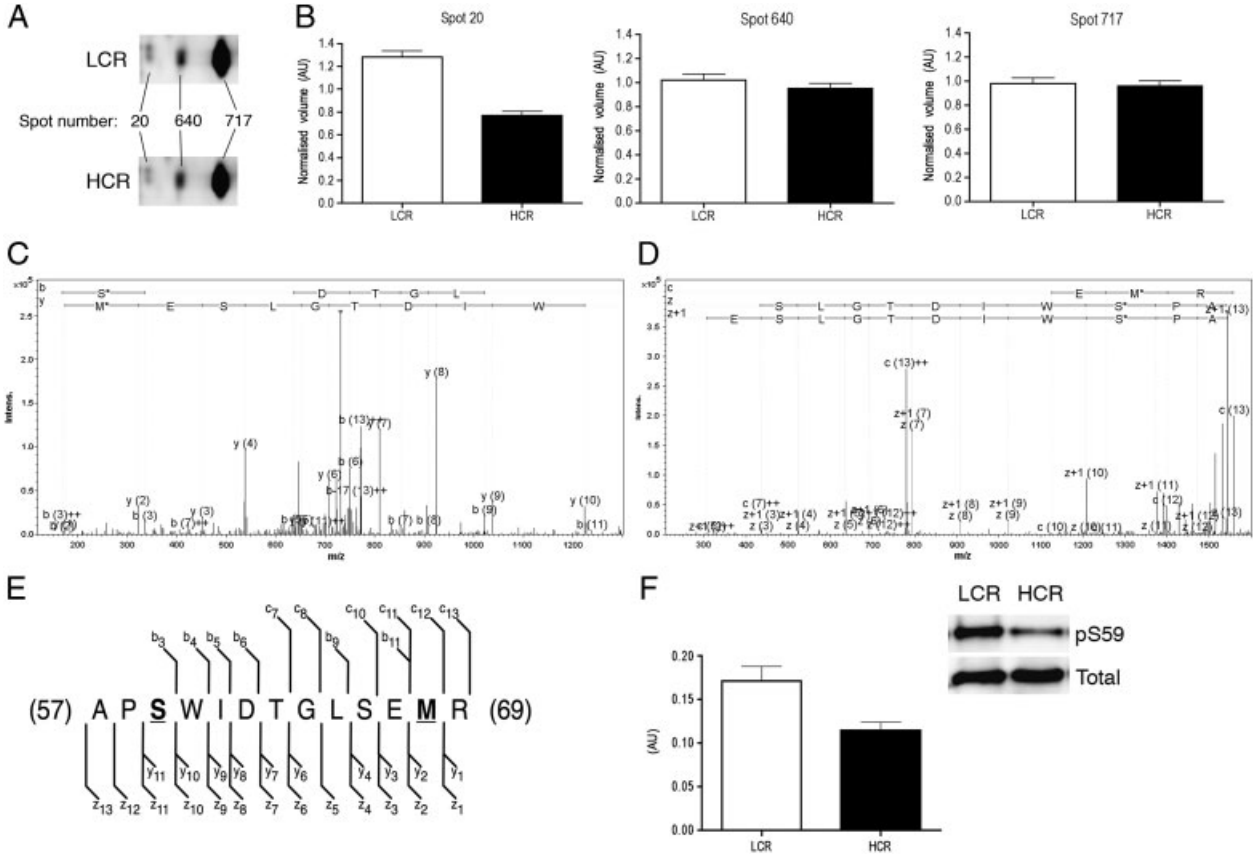

Figure 2. Phosphorylation of α B-crystallin at S59. Spots 20, 640 and 717 were unambiguously identified as α B-crystallin and the expression of spot 20 was 1.67-fold greater in LCR (A and B). nLC-MS/MS detected a doubly charged precursor (*m/z* 779.86) of peptide APSWIDTGLSEMR (residues 57–69) in spot 20 that was not present in spot 640 or spot 717. Site-specific mapping of serine phosphorylation was performed using (C) CID and (D) ETD techniques. (E) Interpretation of fragment ion spectra confirmed oxidation of methionine 68 and phosphorylation of serine 59; bold underlined type denotes modified residues. MOWSE peptide scores from CID and ETD fragmentation were 55 and 80, respectively. (F) Western blot analysis confirmed the ratio of α B-crystallin phosphorylated serine 59 relative to total α B-crystallin was significantly greater (1.49-fold; $p = 0.02$) in LCR hearts.

stress induced by pressure overload increases microtubule density [30], while overexpression of α B-crystallin helps to maintain cardiomyocyte microtubule integrity [31]. Coronin-6 exhibited the greatest difference (4.4-fold greater in LCRs) in abundance between HCRs and LCRs and correlated significantly with high serum insulin levels in LCRs. Coronin proteins cross-link actin filaments [32] and may also interact with microtubules linking this novel discovery with over-representation of microtubule-based processes in LCRs [7]. The role of coronin-6 in cardiac muscle is yet to be described but changes in the expression of coronin 1 are associated with the transition to maladaptive cardiac hypertrophy induced by transgenic overexpression of myotrophin [33]. Changes in microtubule proteins are consistent with elevated oxidative stress [34] and proteasomal dysfunction [35], which may contribute to the development of cardiomyopathy [36]. Accordingly, LCRs exhibited greater expression of proteasome activator complex subunit 1. Cardiac expression of proteasome activator complex subunit 1 is elevated in diabetic cardiomyopathy induced by streptozotocin, and Powell et al [37] report the 11S-activated proteasome, rather than the 26S-proteasome, is associated with the degradation oxidatively modified proteins.

Post-genomic investigations afford comprehensive unbiased analysis that can advance knowledge and generate novel hypotheses. However, despite using sophisticated statistical analyses, the large number of dependent variables often raises concerns regarding false discoveries. Therefore, validation is important. Duplication of proteomic experiments or the inclusion of technical replicates does not provide validation of the biological significance of the original discoveries. Instead, comparison of data across associated biological models is a more relevant approach. Features of the HCR cardiac proteome, including ACADS and MTE-1, were identical to endurance-trained rat hearts [38] and, therefore, may represent key molecular events associated with enhanced aerobic capacity. Similarly, LCRs exhibited molecular features consistent with animal models of cardiomyopathy. For example, Turko and Murad [39] report modulation of β-oxidation enzymes and differential

expression of voltage-dependent anion channel 1 and catalase in hearts of streptozotocin-induced diabetic rats. Faber et al. [40] found differences in desmin and α B-crystallin expression after pressure-induced cardiomyopathy. Bugger et al. [41] report robust down-regulation of enzymes involved in fatty acid oxidation after 20 wk of aortic constriction, and Meng et al. [42] reveal changes in fatty acid metabolism contribute to cardiac hypertrophy and precede the development of hypertension in spontaneously hypertensive rats.

The correspondence between LCRs and models of cardiomyopathy is testament to the importance of low aerobic capacity in the development of disease. Our discoveries support the thesis that, in normal populations, a decline in physical activity resulting in low aerobic capacity is the antecedent of hypertension and overt cardiac dysfunction. In humans, heart failure is a progressive and complex condition involving both inherited and environmental factors that co-occurs with other complicated risks including hypertension, obesity and insulin resistance. Thus, the use of acute models or inbred strains such as spontaneously hypertensive rat is limited. The LCR-HCR model retains genetic complexity. LCRs manifest many of the features associated with metabolic syndrome, and here we show the cardiac proteome of LCRs is exposed to greater oxidative stress and metabolic perturbations that may underlie their diminished cardiac performance. In contrast, despite low levels of habitual physical activity, HCRs appear to be uniquely protected from cardiometabolic disease and demonstrate an enhanced capacity to utilise fatty acids for cardiac work similar to endurance-trained animals. As such, further interrogation of this model may provide additional clues or even reveal the molecular mechanisms that underlie the complexity of low heart function as a precursor to heart failure.

The 2-D DIGE map associated with this work is available at the World -2DPAGE repository, URL: http://world-2dpage.expasy.org/repository/database=0022.

This work was supported by The Institute for Health Research, Liverpool John Moores University (J.G.B., L.G.K. and S.L.B.) and grants R17718 (L.G.K. and S.L.B.) and 5R01DK7720 (C.F.B., S.L.B. and N.Q.) from the National Center for Research Resources of the National Institutes of Health and the Animal Phenotyping Core of the Michigan Metabolomics and Obesity Center.

The authors have declared no conflict of interest.

5 References

[1] Koch, L. G., Britton, S. L., Artificial selection for intrinsic aerobic endurance running capacity in rats. *Physiol. Genomics* 2001, *5*, 45–52.

[2] Carlborg, O., Jacobsson, L., Ahgren, P., Siegel, P., Andersson, L., Epistasis and the release of genetic variation during long-term selection. *Nat. Genet.* 2006, *38*, 418–420.

[3] Wisloff, U., Najjar, S. M., Ellingsen, O., Haram, P. M. et al., Cardiovascular risk factors emerge after artificial selection for low aerobic capacity. *Science* 2005, *307*, 418–420.

[4] Lujan, H. L., Britton, S. L., Koch, L. G., DiCarlo, S. E., Reduced susceptibility to ventricular tachyarrhythmias in rats selectively bred for high aerobic capacity. *Am. J. Physiol. Heart Circ. Physiol.* 2006, *291*, H2933–H2941.

[5] Noland, R. C., Thyfault, J. P., Henes, S. T., Whitfield, B. R. et al., Artificial selection for high-capacity endurance running is protective against high-fat diet-induced insulin resistance. *Am. J. Physiol. Endocrinol. Metab.* 2007, *293*, E31–E41.

[6] Palpant, N. J., Szatkowski, M. L., Wang, W., Townsend,D. et al., Artificial selection for whole animal low intrinsic aerobic capacity co-segregates with hypoxia-induced cardiac pump failure. *PLoS One* 2009, *4*, e6117.

[7] Bye, A., Langaas, M., Hoydal, M. A., Kemi, O. J. et al., Aerobic capacity-dependent differences in cardiac gene expression. *Physiol. Genomics* 2008, *33*, 100–109.

[8] Biesiadecki, B. J., Brand, P. H., Koch, L. G., Britton, S. L., A gravimetric method for the measurement of total spontaneous activity in rats. *Proc. Soc. Exp. Biol. Med.* 1999, *222*, 65–69.

[9] Nelson, M. M., Jones, A. R., Carmen, J. C., Sinai, A. P. et al., Modulation of the host cell proteome by the intracellular apicomplexan parasite *Toxoplasma gondii*. *Infect. Immun.* 2008, *76*, 828–844.

[10] Burniston, J. G., Adaptation of the rat cardiac proteome in response to intensity-controlled endurance exercise. *Proteomics* 2009, *9*, 106–115.

[11] Holloway, K. V., O'Gorman, M., Woods, P., Morton, J. P. et al., Proteomic investigation of changes in human vastus lateralis muscle in response to interval-exercise training. *Proteomics* 2009, *9*, 5155–5174.

[12] Lynen, F., Wieland, O., [beta]-Ketoreductase. In: *Methods Enzymol.* Academic Press, New York, 1955, 566–573.

[13] Burniston, J. G., Changes in the rat skeletal muscle proteome induced by moderate-intensity endurance exercise. *Biochim. Biophys. Acta* 2008, *1784*, 1077–1086.

[14] Liang, X., Le, W., Zhang, D., Schulz, H., Impact of the intramitochondrial enzyme organization on fatty acid oxidation. *Biochem. Soc. Trans.* 2001, *29*, 279–282.

[15] Mayr, M., Chung, Y. L., Mayr, U., McGregor, E. et al., Loss of PKC-delta alters cardiac metabolism. *Am. J. Physiol. Heart Circ. Physiol.* 2004, *287*, H937–H945.

[16] Chu, G., Kerr, J. P., Mitton, B., Egnaczyk, G. F. et al., Proteomic analysis of hyperdynamic mouse hearts with enhanced sarcoplasmic reticulum calcium cycling. *Faseb J.* 2004, *18*, 1725–1727.

[17] Sun, B., Wang, J. H., Lv, Y. Y., Zhu, S. S. et al., Proteomic adaptation to chronic high intensity swimming training in the rat heart. *Comp. Biochem. Physiol. Part D Genomics Proteomics* 2008, *3*, 108–117.

[18] Gerber, L. K., Aronow, B. J., Matlib, M. A., Activation of a novel long-chain free fatty acid generation and export system in mitochondria of diabetic rat hearts. *Am. J. Physiol. Cell Physiol.* 2006, *291*, C1198–C1207.

[19] Goni, F. M., Requero, M. A., Alonso, A., Palmitoylcarnitine, a surface-active metabolite. *FEBS Lett.* 1996, *390*, 1–5.

[20] Finck, B. N., The PPAR regulatory system in cardiac physiology and disease. *Cardiovasc. Res.* 2007, *73*, 269–277.

[21] Makowski, L., Noland, R. C., Koves, T. R., Xing, W. et al., Metabolic profiling of PPARalpha$^{-/-}$ mice reveals defects in carnitine and amino acid homeostasis that are partially reversed by oral carnitine supplementation. *Faseb J.* 2009, *23*, 586–604.

[22] Chen, C. H., Budas, G. R., Churchill, E. N., Disatnik, M. H. et al., Activation of aldehyde dehydrogenase-2 reduces ischemic damage to the heart. *Science* 2008, *321*, 1493–1495.

[23] Zhou, S. G., Wang, P., Pi, R. B., Gao, J. et al., Reduced expression of GSTM2 and increased oxidative stress in spontaneously hypertensive rat. *Mol. Cell. Biochem.* 2008, *309*, 99–107.

[24] Thyfault, J. P., Rector, R. S., Uptergrove, G. M., Borengasser, S. J. et al., Rats selectively bred for low aerobic capacity have reduced hepatic mitochondrial oxidative capacity and susceptibility to hepatic steatosis and injury. *J. Physiol.* 2009, *587*, 1805–1816.

[25] Tweedie, C., Romestaing, C., Burelle, Y., Safdar, A. et al., Lower oxidative DNA damage despite greater ROS production in muscles from rats selectively bred for high running capacity. *Am. J. Physiol. Regul. Integr. Comp. Physiol.* 2010, *300*, R544–R553.

[26] Aggeli, I. K., Beis, I., Gaitanaki, C., Oxidative stress and calpain inhibition induce alpha B-crystallin phosphorylation via p38-MAPK and calcium signalling pathways in H9c2 cells. *Cell Signal.* 2008, *20*, 1292–1302.

[27] Whittaker, R., Glassy, M. S., Gude, N., Sussman, M. A. et al., Kinetics of the translocation and phosphorylation of alphaB-crystallin in mouse heart mitochondria during ex vivo ischemia. *Am. J. Physiol. Heart Circ. Physiol.* 2009, *296*, H1633–H1642.

[28] Launay, N., Goudeau, B., Kato, K., Vicart, P., Lilienbaum, A., Cell signaling pathways to alphaB-crystallin following stresses of the cytoskeleton. *Exp. Cell. Res.* 2006, *312*, 3570–3584.

[29] Pawlak, A., Gil, R. J., Walczak, E., Seweryniak, P., Desmin expression in human cardiomyocytes and selected clinical and echocardiographic parameters in patients with chronic heart failure. *Kardiol. Pol.* 2009, *67*, 955–961.

[30] Cooper, G., Cytoskeletal networks and the regulation of cardiac contractility: microtubules, hypertrophy, and cardiac dysfunction. *Am. J. Physiol. Heart Circ. Physiol.* 2006, *291*, H1003–H1014.

[31] Bluhm, W. F., Martin, J. L., Mestril, R., Dillmann, W. H., Specific heat shock proteins protect microtubules during simulated ischemia in cardiac myocytes. *Am. J. Physiol.* 1998, *275*, H2243–H2249.

[32] Rybakin, V., Clemen, C. S., Coronin proteins as multifunctional regulators of the cytoskeleton and membrane trafficking. *Bioessays* 2005, *27*, 625–632.

[33] Sarkar, S., Leaman, D. W., Gupta, S., Sil, P. et al., Cardiac overexpression of myotrophin triggers myocardial hypertrophy and heart failure in transgenic mice. *J. Biol. Chem.* 2004, *279*, 20422–20434.

[34] Devillard, L., Vandroux, D., Tissier, C., Brochot, A. et al., Tubulin ligands suggest a microtubule-NADPH oxidase relationship in postischemic cardiomyocytes. *Eur. J. Pharmacol.* 2006, *548*, 64–73.

[35] Dong, X., Liu, J., Zheng, H., Glasford, J. W. et al., In situ dynamically monitoring the proteolytic function of the ubiquitin-proteasome system in cultured cardiac myocytes. *Am. J. Physiol. Heart Circ. Physiol.* 2004, *287*, H1417–H1425.

[36] Bulteau, A. L., Lundberg, K. C., Humphries, K. M., Sadek, H. A. et al., Oxidative modification and inactivation of the proteasome during coronary occlusion/reperfusion. *J. Biol. Chem.* 2001, *276*, 30057–30063.

[37] Powell, S. R., Samuel, S. M., Wang, P., Divald, A. et al., Upregulation of myocardial 11S-activated proteasome in experimental hyperglycemia. *J. Mol. Cell. Cardiol.* 2008, *44*, 618–621.

[38] Burniston, J. G., Hoffman, E. P., Proteomic responses of skeletal and cardiac muscle to exercise. *Exp. Rev. Proteomics* 2011, *8*, 361–377.

[39] Turko, I. V., Murad, F., Quantitative protein profiling in heart mitochondria from diabetic rats. *J. Biol. Chem.* 2003, *278*, 35844–35849.

[40] Faber, M. J., Dalinghaus, M., Lankhuizen, I. M., Bezstarosti, K. et al., Proteomic changes in the pressure overloaded right ventricle after 6 weeks in young rats: correlations with the degree of hypertrophy. *Proteomics* 2005, *5*, 2519–2530.

[41] Bugger, H., Schwarzer, M., Chen, D., Schrepper, A. et al., Proteomic remodelling of mitochondrial oxidative pathways in pressure overload-induced heart failure. *Cardiovasc. Res.* 2010, *85*, 376–384.

[42] Meng, C., Jin, X., Xia, L., Shen, S. M. et al., Alterations of mitochondrial enzymes contribute to cardiac hypertrophy before hypertension development in spontaneously hypertensive rats. *J. Proteome Res.* 2009, *8*, 2463–2475.

